Faculty of Engineering

Department of Materials Science and Engineering

MLE4101A BEng Dissertation (PPP)

Materials Discovery for Battery Applications from AI and Computation

Supervisor: Asst. Prof. Pieremanuele Canepa

Chan Yao Kuan (A0182864U)

Introduction

The development of green energy technologies, such as photovoltaics, wind turbines, and rechargeable batteries is essential in meeting the sustainable needs of our societies to limit fossil fuel usage. Lithium (Li)-ion batteries power the world's mobile devices, and they are increasingly seen in vehicular transportations. However, when life-cycle analysis is examined in the design of battery architectures, sodium (Na) appears attractive because it can be extracted directly from the oceans, making Na ~50 times lower in cost than Li. Na-ion batteries also use inexpensive, stainless-steel current collectors.[1][2] However, commercial Li-ion batteries and the state-of-the-art Na-ion batteries utilize highly flammable organic liquid electrolytes, [3] which pose a tangible safety concern in their widespread use and deployment.

The replacement of the presently used liquid electrolytes with a non-flammable solid electrolyte is an important avenue to create safer batteries. The natrium superionic CONductor (NaSiCON) $Na_{1+x}Zr_2Si_xP_{3-x}O_{12}$ ($0 \leq x \leq 3$) discovered by Hong and Goodenough, that displays high bulk ionic conductivity and good stability toward other NaSiCON-based electrodes is a good solid electrolyte in NaSiCON-based batteries.[4][3, 5]

Literature Review

This report will now cover several key papers in the literature that elucidates Modern Computing techniques incorporated in Material Science Theory and in the following order: 1) Computational Analysis and Identification of Battery Materials and 2) Phase Behaviour in the Rhombohedral phases of NaSiCON Electrolytes and Electrodes 3) Fast Na-ion Transport in the NaSiCON-type Skeleton Structures

1. Computational Analysis and Identification of Battery Materials

Material Science today enjoys an exponential growth of computing-processing power which has seen the rise of powerful and wide-ranging computational methods. One such example is in the discovery of new battery materials which will be elaborated on, later in this report. Traditionally, the conventional method to discover such materials has been to synthesize and test a large variety of compounds based on the researcher's experience.[6] Note that the research experience follows typically chemical intuition. Comparatively, modern computational methods boast time efficiency by removing a significant amount of guesswork as they are capable of predicting many properties of materials in general, and batteries specifically, before they are even synthesized in the laboratory.[7] One of the key ideas highlighted in literature is the application of traditional material science fundamentals

to screen large crystal structure databases, which shows promising insight to act as a preliminary screening technique for researchers.[8] Therefore, the computational approach, hand in hand with experimental activities, can only increase the turnover of functional materials and molecules, as amply demonstrated by the *in silico* development pharmaceutical molecules.[9, 10]

A key computational method is Ab Initio Molecular Dynamics (AIMD) Simulation, which aims to incorporate the accuracy of Density Functional Theory (DFT) Quantum Mechanical calculations with the Newton equation of motion, to model accurate phenomena at realistic conditions.[7]As described in literature, AIMD can be applied to iterative computations of velocities and positions of a system resulting in its future trajectory to solve Newton's equation of motion.[11] AIMD simulations of trajectories of ion migrations has been extremely valuable in reproducing mechanisms of Li and Na transport within battery materials and other materials for electrochemical devices. From these simulations, we can reliably determine rate constants and diffusion constants which form the basis of predicting cation translocation efficiency in batteries.[7]

2. Phase Behaviour in Rhombohedral NaSiCON

Existing literature points to a vast amount of research available to optimize Na-ion conductivity within NaSiCON electrolyte particularly at $x \sim 2$ in $Na_{1+x}Zr_2Si_xP_{3-x}O_{12}$.[12] The superionic conductivity in NaSiCON at high temperatures (>450K) is rooted in a Na-vacancy migration mechanism that displaces Na+ ions between two characteristic sites, i.e. Na(1) and Na(2) giving rise to Na-ion transport.[13] **Figure 1** below depicts the crystal structure of the rhombohedral phase of NaSiCON where the blue Oxide tetrahedra share corners with two grey ZrO_6 oxide octahedral which forms the basis of a "Lantern Unit"[5, 12].

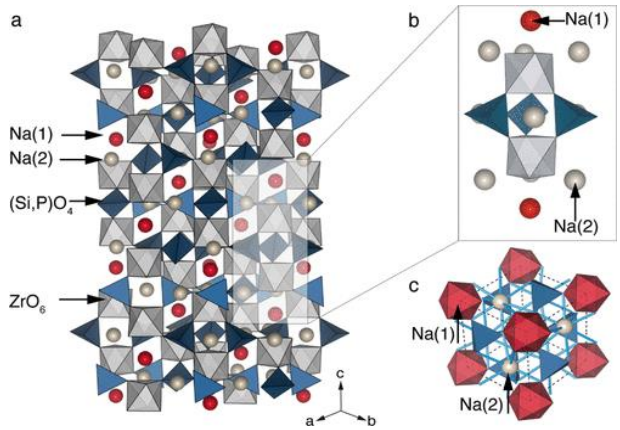

Figure 1: Rhombohedral NaSiCON structure, with the lantern unit on the top right.

The volume of the polyhedral formed by Na(1) site is larger than Na(2) and is coordinated by oxygen atoms from ZrO_6 units. Na(2) resides in an irregular polyhedral, coordinated to seven neighbouring oxygen atoms from the PO_4^{3-} units.[5, 14] An important feature to note is that at temperatures below 450K, NaSiCON undergoes a monoclinic distortion from the rhombohedral $R\bar{3}C$ phase that is attributed with Na+ ions ordering into distinct Na sites and lower Na conductivities.[12] A further example of computational material science using DFT quantum mechanical calculations is observed when researchers described the phase diagram of NaSiCON with varying composition x against temperature.[12]

3. Fast Na + - Ion Transport In Skeleton Structures

To be considered Fast ion transport, the activation energy for an ion to jump from one site to another must be small. At room temperature, NaSiCON structures with formula $Na_{1+x}Zr_2Si_xP_{3-x}O_{12}$, compositions $1.8 < x < 2.2$ distort from rhombohedral structure $R\bar{3}C$ into a monoclinic space group C 2/c.[13] At these compositions, the high Na-ion transport is only achieved at temperature above ~160°C, and enabled by the frustrated rhombohedral $R\bar{3}C$ lattice. In particular, in the subsequent papers published by Hong the same year, it was discovered that the introduction of excess Na+ ions introduces electrostatic Na+ - Na+ interactions that can lower the activation energy even though transport can only occur via Na(1) sites.[5] The paper concludes that transport properties of NaSiCON at 300°C are comparable to that of beta alumina which proves its excellent conductivity and will be the material of primary discussion in the later topics due to the extensive research conducted, and readily available data for benchmarking.

Despite the sizeable share of research on $Na_{1+x}Zr_2Si_xP_{3-x}O_{12}$, it has been observed in numerous studies that Na+ ions struggle to conduct ion-mass transport at temperatures below 160°C which hinders its ability to serve as a viable replacement to Li-ion, and will be the primary concern for this paper.[13]

The primary objective of this project is to use Ab initio Molecular Dynamic Simulation (AIMD), in combination with Density Functional Theory (DFT) and Machine Learning Interatomic Potentials (MLIP), to simulate behaviour of NaSiCON structure at various temperatures to model Na-ion migration mechanism. If this can be achieved accurately, further studies can be conducted via simulations on doping mechanisms to study the effects of Na+ ion transport at room temperature. It should also be noted that MLIP is the method of choice

for two primary reasons. Although AIMD simulations incorporate explicitly the nature of electrons which are computationally most accurate, they are expensive to achieve relevant stochastic descriptions of Na-ion jumps in the NaSICON lattice, which is paramount to accurately describe Na+ ion Transport.[15] Meanwhile, longer simulation times can be achieved with classical potential (Morse, Buckingham, LJ Potentials, etc) molecular dynamics but with erratic accuracy and predictability. Therefore, there is a need for sophisticated and scalable models to bridge the gap between the accuracy of AIMD simulations and inexpensive, but inaccurate molecular dynamics from classical potentials. MLIP is thus the method of choice as it is trained on high-fidelity AIMD but enables longer and more extensive simulations. Having MLIP trained potentials could possibly elucidate new explanations on the highly complex mechanism of Na+ ion transport in disordered NaSiCON structures and other electrolytes of interest.[16]

Methodology

This report will now elaborate on the various software packages used for conducting the simulation experiment. **Figure 2** below shows a summary of all machine learning packages used and the workflow methodology.

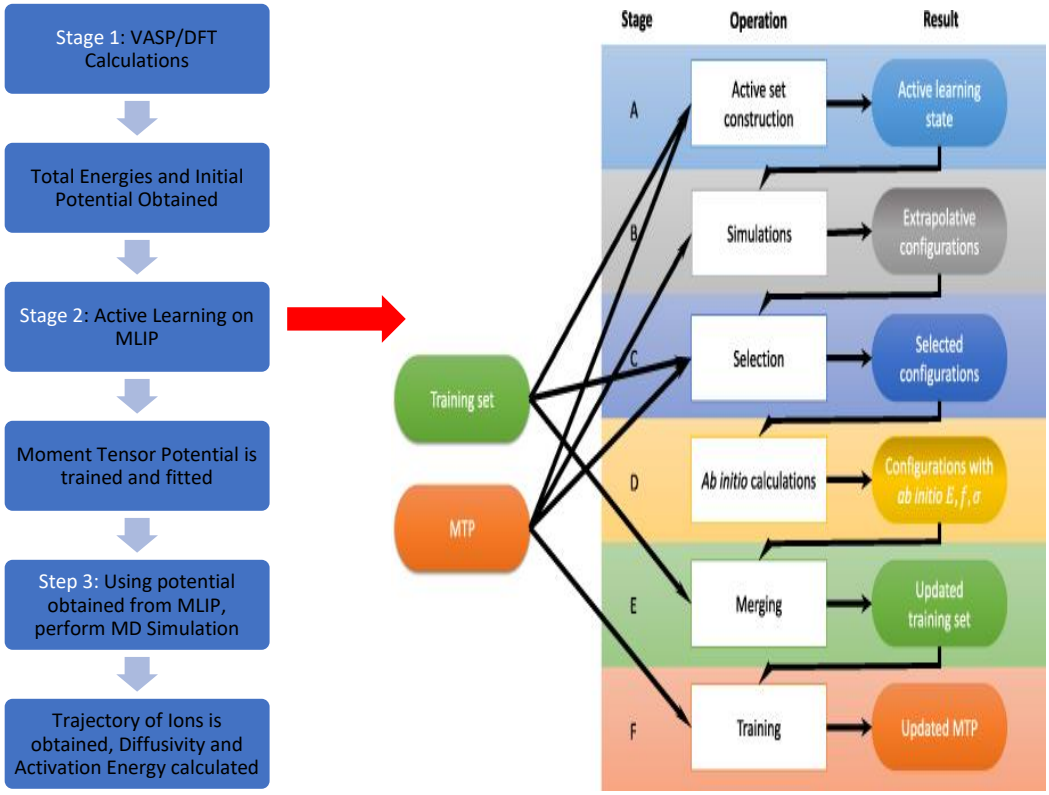

Figure 2: Workflow Overview **(a)** and Active Learning Bootstrap Iterations **(b)**[16]

1. **First-principles Calculations**

One of the leading methods of solving Schrodinger's equation for a system comprising many-ions and many-electrons as a materials is via numerical approaches.[7] A breakthrough was made by Walter Kohn and Liu Sham, who introduced density-functional theory (DFT), which reduces the complexity of electronic many-body interactions to an effective set of single-electron equations when immersed in the field of all other electrons.[17] The mean-field approach used by DFT enables, with some approximation, the simulation of complex materials and molecules at realistic conditions. Here the theory of DFT was used through its implementation in the VASP code[18]which was developed with the intent to offer a set of routines for calculating (and visualizing) from eigenstates, energies and forces across a distributed range of materials properties from atomic, electronic structures to mechanical properties (elastic moduli, theoretical strength) and even thermodynamic properties (activation energies, chemical reactions).

2. **Machine Learning Interatomic Potentials (MLIP)**

Machine-learning interatomic potentials are models to predict potential energy surfaces of interacting atoms as a function of their positions and chemical types.[16] These models differ from empirical models by introducing a functional form that can be iteratively improved to approximate an arbitrary quantum mechanical interaction, subject to some assumptions.[16] Typical MLIP structures consist of Linear Regression with a set of Polynomial Basis Functions. These structures are known as Moment Tensor Potentials (MTP) [16] which are a subclass of MLIP and will be the main focus of this report. MTP potentials represents the energy of an atomic configuration as a sum of contributions of local atomic environments of each atom.

Further expanding on the polynomial functions (Chebyshev polynomials) which introduces two parameters, R_{min} and R_{cut}, which set the cut-off distance between atoms and where they are allowed to interact. This is constructed via *level of moments* (LevMax) which in short, serve as a hyperparameter to our Machine Learning model to represent the complexity of our quantum-mechanical modelling. Another key feature of MTP is in the extrapolation grade, γ_{cfg}. The extrapolation grade seeks to optimize accuracy of the Machine learning model by "interpolating" compared to

"extrapolating".[19] This is achieved by automating selection of the training set, compared to manual selection of training configurations via the extrapolation grade. It should also be noted that interpolating is superior to extrapolating, where the model is going outside the configuration space and would mean less reliable and accurate predictions.[20]

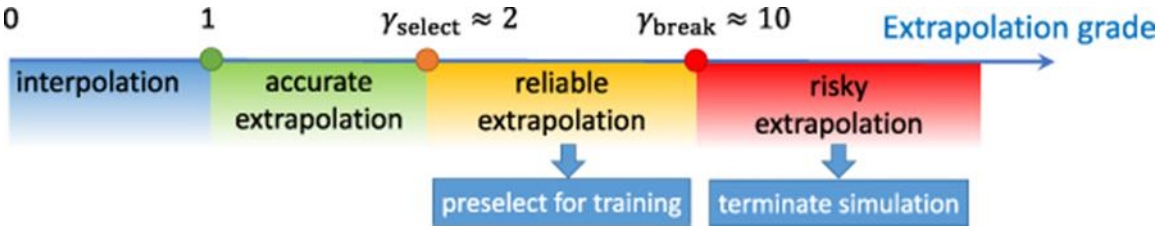

Figure 3: Extrapolation grade used to assess "stability" of configuration[16]

A single iteration of the entire active learning algorithm consists of the following steps (**Figure 2(b)**):

a) On the first step, the active set is selected among all configurations from the training set generated by accurate AIMD simulations and the active learning state is formed.

b) Run the simulation with the current potential and active selection of the extrapolative configurations ($\gamma_{select} > \gamma_{cfg}$). The simulation runs until its successful completion, or until $\gamma_{cfg} > \gamma_{break}$.

c) If a simulation stops after exceeding the maximum allowed extrapolation grade ($\gamma_{cfg} > \gamma_{break}$.), the active-training set is updated. To that end, the $|Volume|$ algorithm is used to select the new configurations to improve the training set and re-train the MLIP model. These new structures are appended to the training set among all extrapolative configurations sampled at the first step.

d) The selected configurations are calculated with accurate DFT model.

e) Next, the selected DFT configurations, their total energy, forces acting on atoms, and stresses, are appended to the trained set.

f) The MTP is retrained.

The iteration of steps (a) to (f) proceed until the simulations are complete without exceeding the critical value of extrapolation γ_{break}. Using this method, we can expect a reliable machine learned potential that can undergo molecular dynamic

simulation at various temperatures to elucidate the trajectory of Na+ ion translocation mechanism.

3. **LAMMPS Molecular Dynamics (MD) Simulation**

The trained MLIP (see point 2) is tested using a general purpose LAMMPS code.[16] In performing Molecular Dynamic Simulation using LAMMPS, we performed long MD simulations on a large supercell structure which would not be possible to replicate using more accurate but computationally expensive AIMD simulations. The MD simulation will be performed at a range of temperatures (300-900K) using the canonical ensemble, NVT (N = Number of atoms, V = Volume of unit cell, T = Temperature)[21] using the Nose'-Hoover thermostat. In these MD simulations, the Newton equation of motion was integrated using the verlet algorithm with a timestep of 1 femtosecond. Using these settings, each simulation was initially equilibrated for 1 nanosecond and data-production simulations were carried out for 6ns. The NaSiCON structures prototype extracted from the models of [12] consist of more than 1,300 atoms and represents the composition $Na_{3.4}Zr_2Si_{2.4}P_{0.6}O_{12}$, which is hypothesized to have large Na-ion transport. Note, these time scales and cell size would be impossible to compute with state-of-the-art AIMD simulations and even on the largest supercomputers. Trajectories from these simulations were then used to compute the Root Mean Square required for diffusivity.

Results and Discussion

Level of Moments	Physical Quantity	Number of Configurations	Average Absolute Difference	RMS absolute Difference
LevMax10	Energy(meV/atom)	38,001	1.295	1.670
LevMax10	Forces (meV/ Å)	12,388,326	83.771	173.82
LevMax12	Energy(meV/atom)	38,147	1.045	1.832
LevMax12	Forces (meV/ Å)	1,2435,922	77.011	161.955
LevMax14	Energy(meV/atom)	38,010	0.891	1.188
LevMax14	Forces (meV/ Å)	1,239,1260	69.847	146.873

Table 1: Errors in Iterative MLIP Training across Different Hyperparameters

With the extrapolation grade explained earlier in the methodology section, at every iteration a new potential is fitted using the iterative bootstrapping method (**Figure 2(b)**). The quality of the new potential is assessed against the accurate AIMD training set using the following

criteria: 1) Root Mean Square Absolute Difference, 2) Average Absolute Difference. The expected tolerance level for RMS absolute difference for Energy/Atom will be within ~20 meV/atom. From **Table 1**, we can conclude that the machine learning fitting are within desired tolerance of 1.67 meV/atom, 1.83 meV/Atom and 1.18meV/Atom for LevMax10, 12 and 14 respectively. It can be concluded that our trained potential reproduced the AIMD data well enough. Furthermore, it can also be noted that while increasing the degree of Chebyshev polynomial, hence the quality of the approximation, from a minimum of LevMax10 to a maximum LevMax14, a marginal increase of accuracy of the trained potential is observed from the reduction in RMS absolute difference in Energy across level of moments (see **Table 1**). However, an increase in quality to LevMax14 can have two undesired effects: i) a sudden increase of the computational resources required for the fit of the machine learning potential, and ii) more pernicious is the risk to create a Machine Learning model which is simply accurate due to overfitting of the data. If a model overfits the training data set, it means that it is not robust at predictions, but simply fits well the training data and the parameter space used to train the model.

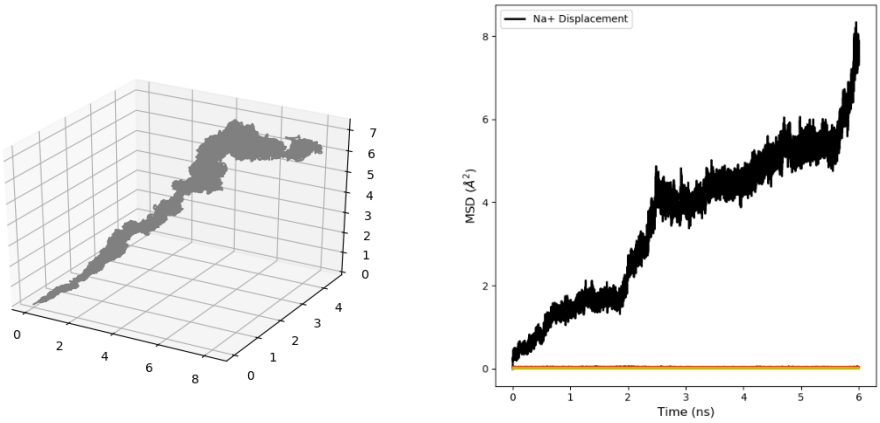

Figure 4: 3D Visualization of Na+ ions Trajectory**(a)**, Mean Squared Displacement(MSD) along [100] at 300K**(b)**

Using a baseline of LevMax10, with the potential obtained from MTP calculated during the active learning step, the cartesian coordinates of Na+ ions at 300K are obtained and plotted as 3-Dimensional figure in **Figure 4a**. Using the same cartesian coordinates of Na-ion as time progresses, the mean square displacement (MSD) of the moving species defined as $\langle r_i(t)^2 \rangle$, i.e. Na-ion is calculated and plotted along [100] axis where the black line represents Na-ion displacement, whereas the other colours represent O, P, Si, and Zr. These computational results

obtained clearly demonstrate that the mobility of Na-ion in the NaSiCON lattice is superior to all the other chemical species (i.e., P, Si, Zr and O). This information complements the experimental notion found in literature, where at 300K, Na+ ions are the only species giving rise to diffusion.[12, 14, 22-25]

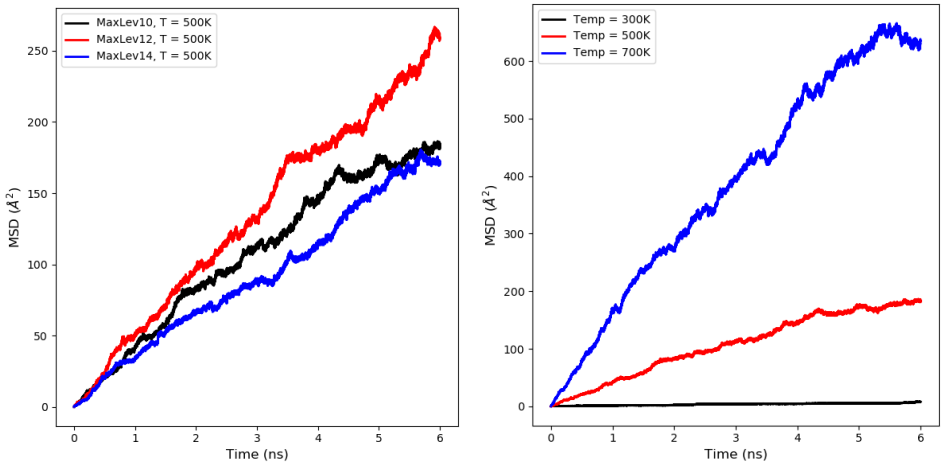

Figure 5: MSD obtained at different level of accuracy for the rhombohedral NaSiCON phase at 500K**(a)**, MSD of MaxLev10 for the rhombohedral phase at 300,500,700K.**(b)**

Based on the results obtained in **Figure 5(a)**, we can again conclude that different degrees of polynomials used in LevMax10, 12 and 14 are consistent with each other, and their trained potentials do not differ significantly. Next, we can conclude based on the MSD of Na-ions at different temperatures **(Figure 5(b))**, that at higher temperatures, Na+ ions diffuse over a larger distance because of the increased diffusivity which will be discussed below.

The formalism to explain the macroscopic diffusivity of Na-ion in NaSiCON is defined by Fick's first law of diffusion (**Equation 1.)**

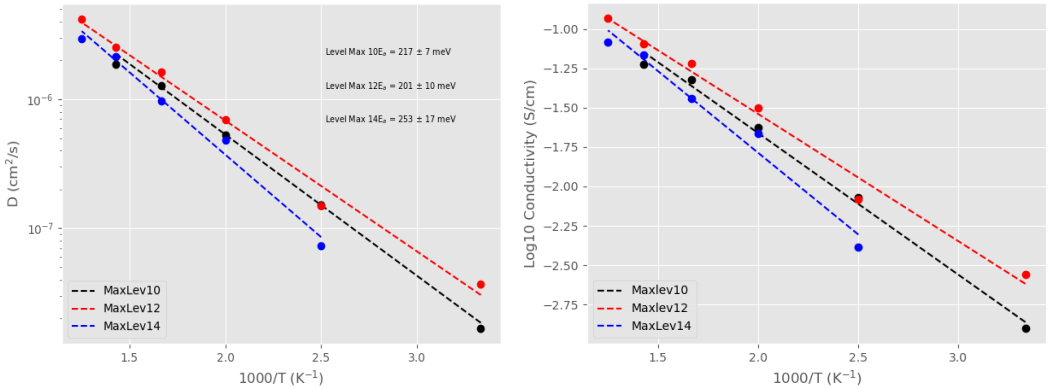

Figure 6: Arrhenius relationship of Diffusivity of Rhombohedral phase**(a)**, Arrhenius relationship of Conductivity of Rhombohedral phase**(b)**

Equation 1: Fick's First Law of Diffusion	$J = -D_{\mathrm{Na}} \frac{d\mu}{dx}$
Equation 2: Self Diffusion of Na Data from MSD	$\langle r_i(t)^2 \rangle = 6\, D_{Na}\, t$
Equation 3: Arrhenius Equation	$D_{Na} = D_0\, exp \frac{-E_a}{K_b T}$
Equation 4: Nernst – Einstein Equation	$\sigma = D_{Na} * H_R * \frac{nq}{K_b T}$

Table 2: Table Of Equations

From Fick's First Law of Diffusion (**Equation 1**), which relates the concentration gradient of a chemical species, $\frac{d\mu}{dx}$ to its flux J, to describe the ion mobility, the chemical diffusion coefficient. At the atomistic level, the chemical diffusion coefficient may be described using D_{Na}, which is related to the MSD obtained from the MD Simulation through **Equation 2** above.[26] By using **Equation 2** where $\langle r_i(t)^2 \rangle$ represents the MSD and *t* represents the timestep (here 1 femtosecond), we are able to obtain Diffusivity D_{Na} in units of cm^2 /s. Then, using the Arrhenius equation (**Equation 3),** we obtain our Activation Energy, Ea in meV where D_0 is the Diffusion coefficient and K_b would be the Boltzmann constant.

Therefore, by plotting log of **Equation 3** versus the inverse of temperature, we can extract the activation energy Ea required for Na to diffuse between each Na site. (**Figure 6(a**))

Finally, we used the solid-state diffusion coefficients D_{Na} to estimate bulk Na-ion conductivities according to the Nernst- Einstein equation (**Equation 4**) described above where K_b denotes Boltzmann's constant, q the elementary charge of the mobile ions, n to the number density of charge carriers, and H_R, the haven ratio, is taken to be equal to 1.

Specifically, in our simulations, the number density of Na+ ions were calculated in the initial configuration of x = 2.4 or the equivalent of 216 number of Sodium atoms. Then, the volume of the unit cell was calculated to be 4466 in $Å^3$, which is then converted to cm^3. The Nernst – Einstein equation was applied to each temperature step to obtain the plot seen in **Figure 6(b)** above.

Up until now, we have only discussed the conductivity and diffusivity of NaSiCON in the rhombohedral phase, by applying the same steps as above to a separate initial configuration in the monoclinic phase, and combining both results in the same plot, we obtain **Figure(s) 7** below.

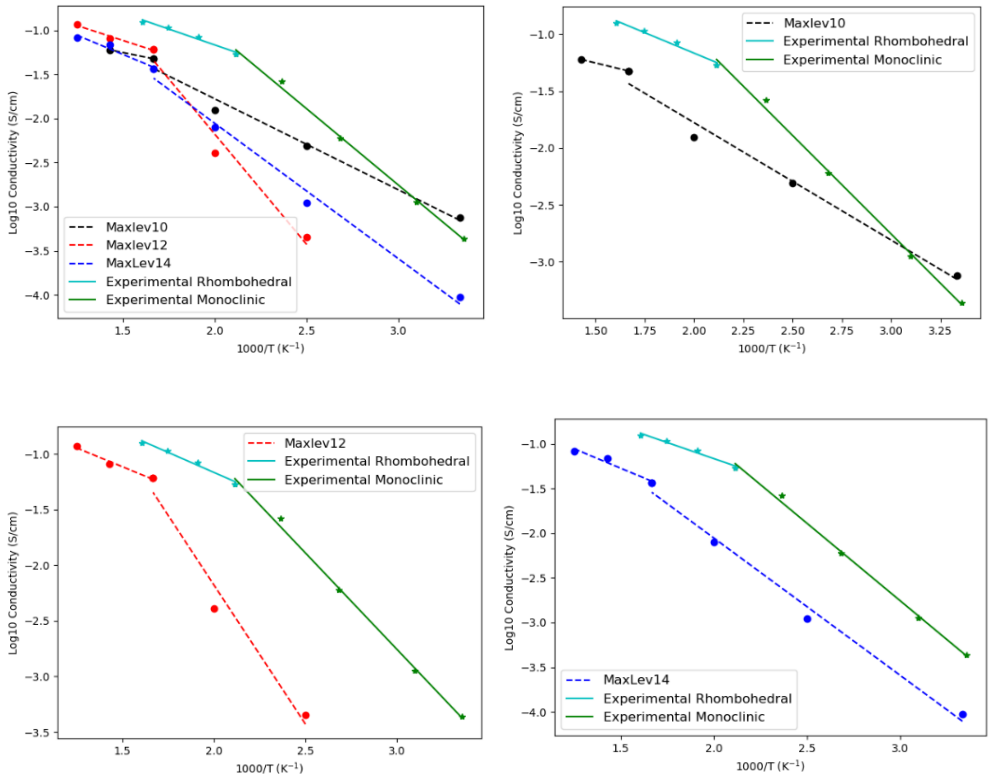

Figure(s) 7: All Computed Conductivities **(a)**, Computed Conductivity MaxLev10 **(b)**, Computed Conductivity MaxLev12 **(c)**, Computed Conductivity MaxLev14 **(d)** , (Top left **(a)** to bottom right**(d)**)

Ionic Conductivity in materials is typically extracted from electrochemical impedance spectroscopy[14, 22], therefore our computed ionic conductivity results may be compared like-for-like with experimental data where x =2.4 (and Na = 3.4), which matches our configuration, seen above in the green and cyan lines which represent Monoclinic and Rhombohedral phase respectively.

Activation Energy (meV)	**LevMax10**	**LevMax12**	**LevMax14**	**Experimental Data**	**Phase**
Ea(meV)	248.1	386.3	284.1	380	Monoclinic
Ea(meV)	217.1	201.1	253.4	220	Rhombohedral

Table 3: Computed and Experimental Activation Energies

By comparing Activation Energies across our simulations (LevMax10, 12 and 14) with experimental data in **Table 3**, we observe that LevMax12 has the closest activation energy compared to experimental data for the monoclinic phase, while LevMax10 is closest in the rhombohedral phase. Across all simulations, the monoclinic and rhombohedral phase are consistent with each other in that the monoclinic phase, stable at lower temperatures, display a higher Activation energy than the rhombohedral. This suggests Na atoms have a larger activation barrier for diffusion to occur at lower temperatures, which is in excellent agreement with experimental literature.[14, 22, 23, 26]

By comparing **Figure(s) 7(b-d)**, it may be observed that by increasing degree of polynomials used in MLIP, the trained potential sees a higher level of accuracy, as seen by comparing LevMax10, 12 and 14 against experimental data individually, where LevMax14 has a closer fit in terms of graph shape with experimental data. It can also be noted that all simulations have consistently lower conductivities than recorded experimental data. This underestimation of ionic conductivity can be attributed to overfitting during the MLIP active learning[16], or suggests DFT calculations were not of high enough fidelity.[15]

Lastly, it may also be noted that all simulations are able to reproduce behaviour of both rhombohedral and monoclinic phase well, as seen in all graphs where at ~ 571K, there is a steep decrease in gradient, which signifies a phase transition from rhombohedral to monoclinic which is well captured. This behaviour could be explained as the phase transition from rhombohedral to monoclinic is associated with Na+ ordering into distinct Na sites and lower conductivities, which explains the increase in activation energies at the monoclinic phase.[12]

Discussion of Na+ Ion Mechanism(s) in NaSiCON

1. **Diffusion Pathways**

   The Na+ diffusion mechanism has been studied by both experimental and computational techniques to investigate the Na+ diffusion pathways. In a similar experiment conducted, researchers computationally doped NaSiCON with Scandium and then conducted similar AIMD simulations as above to yield results in **Figure 8**.[22]The plot on the left via MD simulations plots the trajectories of the accumulated Na+ ions over the simulation time, which reveals via MD simulation the migration pathways and regions in the lattice most frequently traversed by Na+ ions. Such 3D

diffusion behaviour of Na+ ions allows access to all possible pathways and helps to enhance the ionic conductivity.[22]

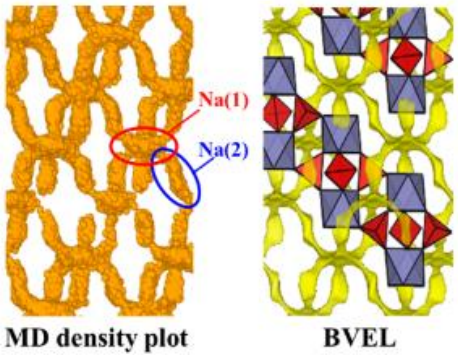

Figure 8: MD Simulation at 473K for total 1 ns, performed by [22]

2. **Na(1) – Na(2) Site Exchange**

As mentioned in the literature review, the rhombohedral NaSiCON form has two different crystallographic Na sites. The local Na-Na environment where each Na(1) site is surrounded by 6 Na(2) sites and each Na(2) site is surrounded by 2 Na(1) sites would mean most Na migration occurs between Na(1) and Na(2) sites.[12] Researchers have verified such conclusions computationally by examining MD density plots in **Figure 9** below.

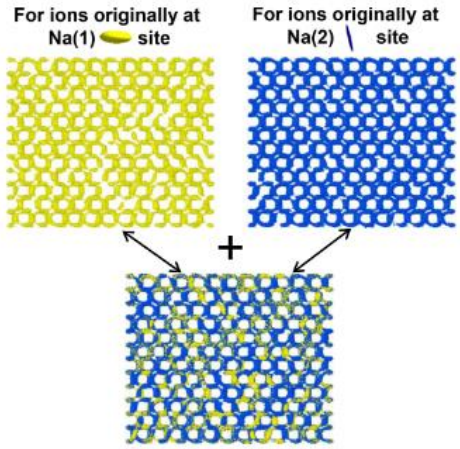

Figure 9: Na+ Ion density from MD Simulation at 473K for Na(1) on the left and Na(2) on the right with a combined overlay(bottom)

In the above plot, the atomistic trajectory was recorded separately for Na+ ions according to their initial site, and the density plots at the beginning of the MD simulation was plotted. As shown, when the two density plots are overlaid on top of

each other, they are very similar and form well-connected 3D pathways between the Na(1) and Na(2) sites.[22]

3. **Na+ Ion Intersite Hopping**

   Finally, by plotting the radial distribution functions (using the van Hove correlation) with different time interval values (**Figure 10**), researchers were able to obtain insights into the time dependence of the Na+ ion diffusion process. The van Hove correlation function starts to form a peak at 3.5 Å in the red line, indicating that the site exchange between Na(1) and Na(2) sites can occur within a very short time scale. As the time interval value increases, Na+ ions are able to accomplish the two-step migration process (Na(1)→Na(2)→Na(1) or Na(2)→Na(1)→Na(2)), resulting in a decrease of intensity of the peak at 3.5 Å, but an increase of intensity of the peaks at 5 and 6.5 Å. Researchers were able to conclude the overall picture of Na+ ion translocation is of short-range hopping between Na(1) and Na(2) sites on a time scale of a few hundred picoseconds, and long-range hopping on time scales of nanoseconds. [22]

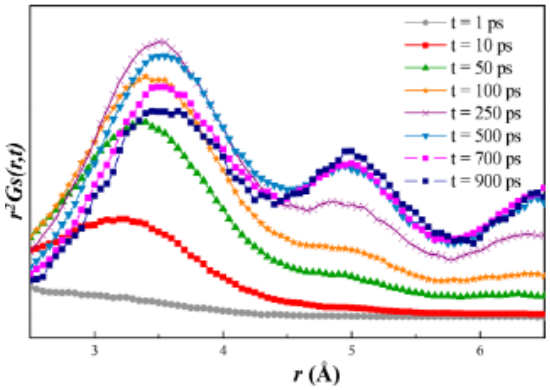

Figure 10: Na+ ion dynamics simulated at 773K on different timescales, y-axis represents probability of moving distance r.

Conclusion

In summary, through this computational exercise, it can be seen that there is a great significance in computational material science, especially for complex systems like the quinary NaSiCON material, where synthesis of the material could take a significant time to produce in a lab with much deviation.[24] After refinement of this computational experiment, with a MLIP model trained on NaSiCON, other researchers would be able to utilize this model to conduct other simulations perhaps on doping mechanisms, such that other behaviour of NaSiCON may be elucidated. A breakthrough would have been made when NaSiCON is able to serve as a viable

replacement to Li-Ion at room temperature. To conclude, there is much more research to be conducted in this new and exciting field.

References

[1] S.-W. Kim, D.-H. Seo, X. Ma, G. Ceder, and K. Kang, "Electrode Materials for Rechargeable Sodium-Ion Batteries: Potential Alternatives to Current Lithium-Ion Batteries," *Advanced Energy Materials,* vol. 2, no. 7, pp. 710-721, 2012, doi: 10.1002/aenm.201200026.

[2] I. Hasa *et al.*, "Challenges of today for Na-based batteries of the future: From materials to cell metrics," *Journal of Power Sources,* vol. 482, p. 228872, 2021, doi: 10.1016/j.jpowsour.2020.228872.

[3] J. Janek and W. G. Zeier, "A solid future for battery development," *Nature Energy,* vol. 1, no. 9, p. 16141, 2016, doi: 10.1038/nenergy.2016.141.

[4] J. B. Goodenough and Y. Kim, "Challenges for Rechargeable Li Batteries," *Chemistry of Materials,* vol. 22, no. 3, pp. 587-603, 2010, doi: 10.1021/cm901452z.

[5] H. Y. P. Hong, "Crystal structures and crystal chemistry in the system Na1+xZr2SixP3−xO12," *Materials Research Bulletin,* vol. 11, no. 2, pp. 173-182, 1976, doi: 10.1016/0025-5408(76)90073-8.

[6] A. Jahan, M. Y. Ismail, S. M. Sapuan, and F. Mustapha, "Material screening and choosing methods – A review," *Materials & Design,* vol. 31, no. 2, pp. 696-705, 2010, doi: 10.1016/j.matdes.2009.08.013.

[7] T. N. F. Meutzner, M. Zschornak, P. Canepa, G. S. Gautam, S. Leoni, S. Adams, T. Leisegang, V. A. Blatov and D. C. Meyer, "Computational analysis and identification of battery materials," 2018.

[8] L. M. Mayr and D. Bojanic, "Novel trends in high-throughput screening," *Current Opinion in Pharmacology,* vol. 9, no. 5, pp. 580-588, 2009, doi: 10.1016/j.coph.2009.08.004.

[9] I. M. Kapetanovic, "Computer-aided drug discovery and development (CADDD): In silico-chemico-biological approach," *Chemico-Biological Interactions,* vol. 171, no. 2, pp. 165-176, 2008, doi: 10.1016/j.cbi.2006.12.006.

[10] Y. Cha *et al.*, "Drug repurposing from the perspective of pharmaceutical companies," *British Journal of Pharmacology,* vol. 175, no. 2, pp. 168-180, 2018, doi: 10.1111/bph.13798.

[11] S. Adams and J. Swenson, "Predictability of ion transport properties from the structure of solid electrolytes," *Ionics,* vol. 10, no. 5-6, pp. 317-326, 2004, doi: 10.1007/bf02377990.

[12] Z. Deng *et al.*, "Phase Behavior in NaSiCON Electrolytes and Electrodes," American Chemical Society (ACS), 2020.

[13] J. B. Goodenough, H. Y. P. Hong, and J. A. Kafalas, "Fast Na+-ion transport in skeleton structures," *Materials Research Bulletin,* vol. 11, no. 2, pp. 203-220, 1976, doi: 10.1016/0025-5408(76)90077-5.

[14] Z. Z. Zhizhen Zhang, Kavish Kaup, Ruijuan Xiao, Siqi Shi,* Maxim Avdeev,*, D. W. Yong-Sheng Hu, Bing He, Hong Li, Xuejie Huang, Linda F. Nazar,*, and a. L. Chen, "Correlated Migration Invokes Higher Na+-Ion Conductivity

in NaSICON-Type Solid Electrolytes," *Advanced Energy Materials,* 2019.

[15] G. A. B. Brajesh K Rai "Fast and accurate generation of ab initio quality atomic charges using nonparametric statistical regression," 2013.

[16] K. G. Ivan S Novikov1, 2, Evgeny V Podryabinkin1and Alexander V Shapeev, "The MLIP package: moment tensor potentials with MPI and activelearning," *Machine Learning Science and Technology,* 2020.

[17] W. Kohn and L. J. Sham, "Self-Consistent Equations Including Exchange and Correlation Effects," *Physical Review,* vol. 140, no. 4A, pp. A1133-A1138, 1965, doi: 10.1103/physrev.140.a1133.

[18] G. Kresse and J. Furthmüller, "Efficient iterative schemes for ab initio total-energy calculations using a plane-wave basis set," *Physical Review B,* vol. 54, no. 16, pp. 11169-11186, 10/15/ 1996, doi: 10.1103/PhysRevB.54.11169.

[19] E. V. Podryabinkin and A. V. Shapeev, "Active learning of linearly parametrized interatomic potentials," *Computational Materials Science,* vol. 140, pp. 171-180, 2017, doi: 10.1016/j.commatsci.2017.08.031.

[20] Z. Li, J. R. Kermode, and A. De Vita, "Molecular Dynamics with On-the-Fly Machine Learning of Quantum-Mechanical Forces," *Physical Review Letters,* vol. 114, no. 9, 2015, doi: 10.1103/physrevlett.114.096405.

[21] D. J. Evans and B. L. Holian, "The Nose–Hoover thermostat," *The Journal of Chemical Physics,* vol. 83, no. 8, pp. 4069-4074, 1985, doi: 10.1063/1.449071.

[22] Y. Deng *et al.*, "Crystal Structures, Local Atomic Environments, and Ion Diffusion Mechanisms of Scandium-Substituted Sodium Superionic Conductor (NASICON) Solid Electrolytes," *Chemistry of Materials,* vol. 30, no. 8, pp. 2618-2630, 2018, doi: 10.1021/acs.chemmater.7b05237.

[23] K. Nakano, N. Tanibata, H. Takeda, R. Kobayashi, M. Nakayama, and N. Watanabe, "Molecular Dynamics Simulation of Li-Ion Conduction at Grain Boundaries in NASICON-Type LiZr2(PO4)3 Solid Electrolytes," *The Journal of Physical Chemistry C,* 2021, doi: 10.1021/acs.jpcc.1c07314.

[24] B. Singh *et al.*, "A chemical map of NaSICON electrode materials for sodium-ion batteries," *Journal of Materials Chemistry A,* vol. 9, no. 1, pp. 281-292, 2021, doi: 10.1039/d0ta10688g.

[25] X. Zhao, Z. Zhang, X. Zhang, B. Tang, Z. Xie, and Z. Zhou, "Computational screening and first-principles investigations of NASICON-type LixM2(PO4)3 as solid electrolytes for Li batteries," *Journal of Materials Chemistry A,* vol. 6, no. 6, pp. 2625-2631, 2018, doi: 10.1039/c7ta08968f.

[26] J. A. Dawson, P. Canepa, T. Famprikis, C. Masquelier, and M. S. Islam, "Atomic-Scale Influence of Grain Boundaries on Li-Ion Conduction in Solid Electrolytes for All-Solid-State Batteries," *Journal of the American Chemical Society,* vol. 140, no. 1, pp. 362-368, 2018, doi: 10.1021/jacs.7b10593.